Soft Nanotubes with a Hydrophobic Channel Hybridized with Au Nanoparticles: Photothermal Dispersion/Aggregation Control of C60 in Water

Kazuyuki Ishikawa, Naohiro Kameta, Masaru Aoyagi, Masumi Asakawa, and Toshimi Shimizu*

Simple glycolipid *N*-alkaroyl-β-D-glucopyranosylamine 1(n) selectively self-assembles into sheets in water, nanotubes in alcohols, and helical nanocoils in toluene. All self-assemblies consist of bilayer membranes in which 1(n) packed in an interdigitated fashion. The outer surface of the sheet is covered with the hydrophilic glucose headgroup of 1(n), whereas those of the nanotube and helical nanocoil are covered with the hydrophobic alkyl-chain tail of 1(n). Heat treatment of the nanotube in the presence of water induces a rearrangement of the molecular packing of the outermost surface that allows the nanotube to become an effective nanocontainer for the dispersion of fullerene (C60) in water, a result of the ability of the hydrophilic outer surface of the nanotube and the hydrophobic nanochannel to encapsulate C60. The nanotube also exhibits photothermal characteristics after being hybridized with Au nanoparticles (AuNPs). The photothermal effect of the AuNPs allows the nanotube to unfold its tubular morphology and leads to compulsive release of the encapsulated C60 to the bulk water. Application of other nanotubes with similar photostimulated transformation ability should facilitate control of the dispersion/aggregation of other carbon nanomaterials, functional aromatic compounds, and drugs with low solubility in water.

1. Introduction

Dispersion control of carbon nanomaterials has been an important issue in various applications, including construction of drug-delivery systems, sensors, and other devices, because aggregation and bundle formation by strong van der Waals interactions cause the solubility of carbon nanomaterials to be low. Recent developments in the field of stimuli-responsive polymeric dispersants have attracted much attention as a possible way to resolve this issue.[1–7] Although light is a great external stimulus in terms of remote and accurate control, rapid switching, and ease of focusing, examples of the introduction of photoresponsive ability to polymeric dispersants are still limited.[8–10]

Non-covalently bonded polymer nanotubes, so-called "supramolecular nanotubes",[11] are formed by self-assembly of well-designed amphiphiles in solvents and are potential candidates as nanocontainers for the dispersion of carbon nanomaterials. Nanotubes are able to not only encapsulate low-molecular-weight molecules (e.g., drugs), biomacromolecules (e.g., DNA and proteins), and nanoparticles in nanochannels with inner diameters of 5–100 nm, but also release those guests to bulk media.[12–15] To act as nanocontainers for the dispersion of carbon nanomaterials in water, nanotubes require a hydrophilic outer surface and a hydrophobic nanochannel. In the past, however, nanotubes have had a hydrophilic outer surface and nanochannel or a hydrophobic outer surface and nanochannel, the former being prepared in water (or organic solvents with high polarities) and the latter in organic solvents with low polarities. Furthermore, control over the storage and release of guests through photostimulation has been reported only in the case of our photoresponsive nanotube,[16] which is composed of an amphiphile modified with an azobenzene moiety as a photoisomerization unit; in response to irradiation, this nanotube is able to instantly release hydrophilic guests encapsulated in the hydrophilic nanochannel to the bulk water while the nanochannel shrinks.

Herein, we investigated in various solvents the self-assembly and thermal-phase transition behavior of simple glycolipids **1(n)** (**Scheme 1**) to form constructed nanotubes that were able to disperse fullerene (C60) in water. To achieve photoresponsive dispersion/aggregation control of C60, we selectively hybridized Au nanoparticles with photothermal behavior to the open end of the nanotubes. We describe the release and aggregation of C60 via photothermally stimulated unfolding from tubular to the fibrous morphology.

Dr. K. Ishikawa, Dr. M. Aoyagi, Dr. M. Asakawa, Dr. T. Shimizu
Nanotube Research Center (NTRC)
National Institute of Advanced Industrial Science and Technology (AIST)
Tsukuba Central 5, 1-1-1 Higashi, Tsukuba, Ibaraki 305-8565, Japan
Dr. N. Kameta
Nanotube Research Center (NTRC)
National Institute of Advanced Industrial Science and Technology (AIST)
Tsukuba Central 5, 1-1-1 Higashi, Tsukuba, Ibaraki 305-8565, Japan
E-mail: n-kameta@aist.go.jp

DOI: 10.1002/adfm.201202160

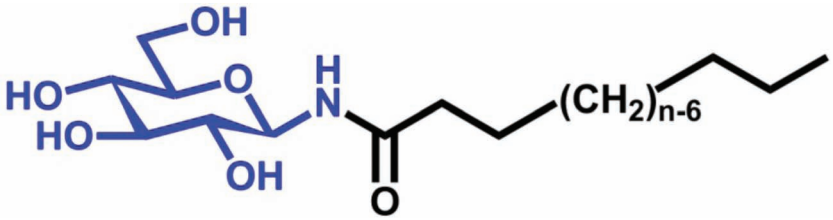

Scheme 1. Chemical structure of the glycolipids **1(n)**, n = 12, 14, 16, and 18.

2. Formation of Nanotubes by Self-Assembly in Various Solvents

Self-assembly experiments were carried out by refluxing **1(n)** (1 mg) in either water, methanol, ethanol, *n*-propanol, *n*-butanol, or toluene (1 mL) for 1 h. The hot solutions were gradually cooled to room temperature. Scanning electron microscopic (SEM) observations revealed that **1(18)** independently formed sheets in water, nanotubes in alcohols, and helical nanocoils in toluene **(Figure 1)**. Consideration of size distributions indicates that the inner diameters, membrane thicknesses, and lengths of all nanotubes formed in a particular alcohol were similar. The alkyl-chain length of **1(n)** influenced self-assembled morphologies. Self-assembly of **1(12)**, **1(14)**, and **1(16)** in methanol and ethanol gave mainly nanotubes, whereas self-assembly of **1(12)**, **1(14)**, and **1(16)** in other solvents gave mixtures of amorphous structures, sheets, helical nanocoils, nanotapes, and nanotubes with different inner diameters (Supporting Information, Figure S1–S3).

Infrared (IR) absorption, powder X-ray diffraction (XRD), and circular dichroism (CD) spectroscopic measurements enabled us to analyze the molecular packing of the self-assemblies. The conformations of the alkyl chain of **1(18)** in the self-assemblies were assignable to an all-*trans* conformation based on the fact that the $\nu_s(CH_2)$ IR stretching bands of all self-assemblies appeared at 2848–2850 cm^{-1} (Supporting Information, Table S1).[17,18] The wavenumbers of the $\delta(CH_2)$ scissoring bands (1473 and 1463 cm^{-1}) and the $\gamma(CH_2)$ rocking bands (731 and 720 cm^{-1}) also suggest that the lateral packing of the alkyl chain of **1(18)**, the so-called "subcell structure", was an orthorhombic perpendicular type (O⊥) (Supporting Information, Table S1).[19,20] The fact that the XRD patterns of all self-assemblies show a single diffraction peak in the small angle region reflects the long *d* spacing of bilayer membranes. Because the *d* value (4.4–4.8 nm) of **1(18)** was smaller than twice the molecular length (L = 3.0 nm), **1(18)** should pack in an interdigitated fashion within the bilayer membranes,[21] a conclusion that is strongly supported by the subcell structure (**Figure 2** left). However, the intermolecular interaction within the bilayer membranes differed among the self-assemblies. The hydrogen bond of **1(18)** was stronger in the sheet morphology than in the nanotube and helical nanocoil configurations, because the amide-I band occurred at a lower wavenumber in the former than in the latter two (Supporting Information, Table S1). Furthermore, there was a stronger negative cotton effect at 200–210 nm in the CD spectra of the nanotube and helical nanocoil compared with the sheet (Supporting Information, Figure S4). The amplification of the cotton effect reflects the contribution of chirality-induced self-assembly,[22,23] which, based on elasticity theory, is known to induce twisting or coiling of the bilayer membranes.[24–26]

3. Surface Properties of Nanotubes

The sheets, nanotubes, and helical nanocoils that self-assembled from **1(18)** in various solvents were all interdigitated within the bilayer membranes, although the intermolecular hydrogen bond strength and chiral packing contribution were different among the self-assemblies. The surface properties of sheets formed in water were completely opposite to those of nanotubes and helical nanocoils formed in alcohols and

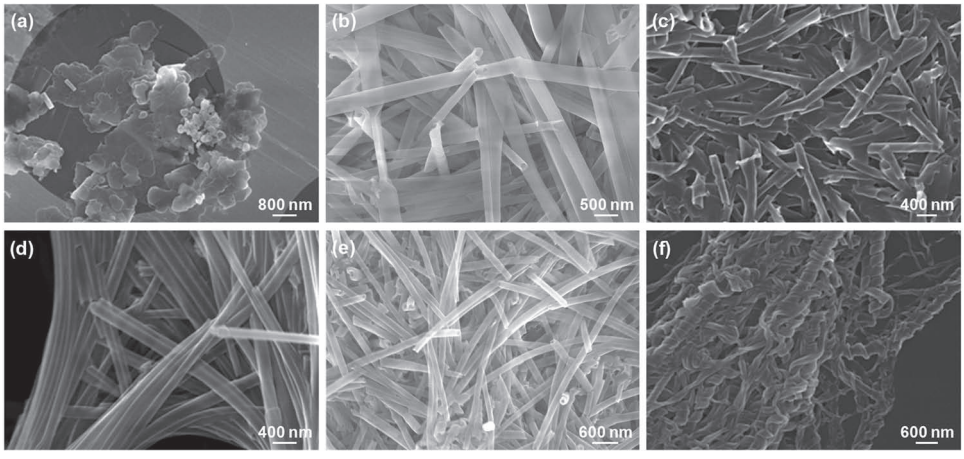

Figure 1. SEM images of the self-assembled morphologies formed from **1(18)** in various solvents. a) The sheets in water, b) nanotubes with 68 ± 17 nm i.d. in methanol, c) nanotubes with 56 ± 15 nm i.d. in ethanol, d) nanotubes with 67 ± 17 nm i.d. in *n*-propanol, e) nanotubes with 83 ± 15 nm i.d. in *n*-butanol, and f) helical nanocoils in toluene.

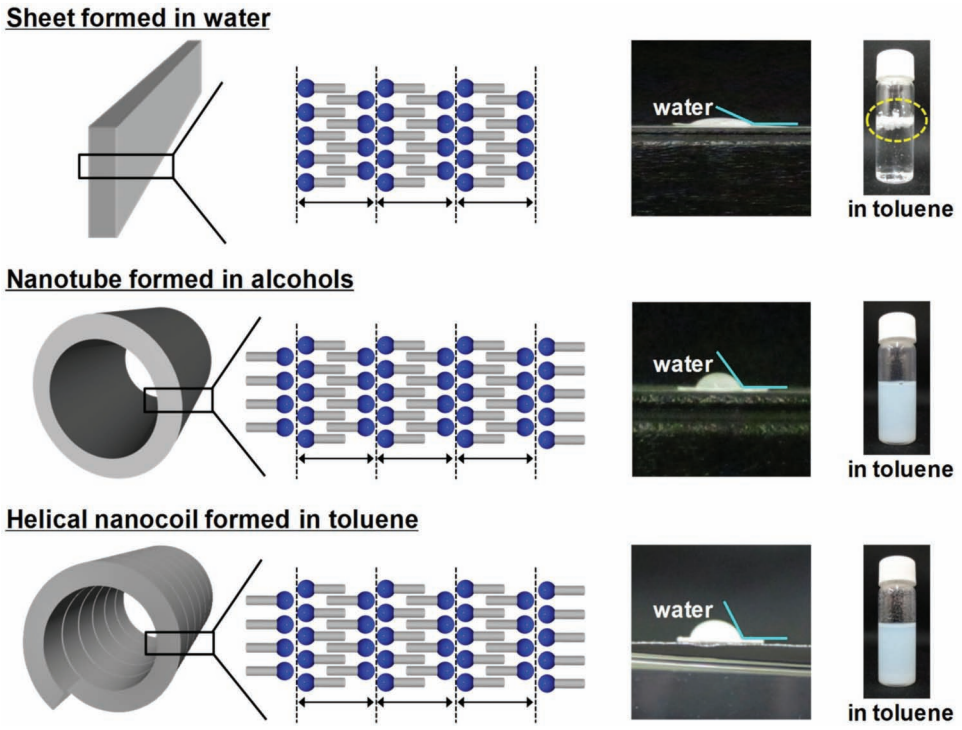

Figure 2. The interdigitated molecular packing within the bilayer membranes of the self-assembled structures (left: schematic images). The contact angle of the pelleted self-assembled structures (middle photographs). The dispersion ability of the self-assembled structures in toluene (right: photographs).

toluene, respectively. The higher contact angles of water on the pelleted nanotubes and pelleted helical nanocoil imply that both self-assemblies have hydrophobic surfaces covered with the alky-chain tail of **1(18)** (Figure 2 middle). In fact, the nanotubes were able to disperse into toluene and *n*-heptane as easily as the helical nanocoil (Figure 2 right). In contrast, the lower contact angles of water and the lower dispersion ability of the sheet into toluene and *n*-heptane suggest that its hydrophilic surface was covered with the glucose headgroups of **1(18)**. A similar tendency has been observed in self-assemblies consisting of bilayer membranes without interdigitated molecular packing, which are formed by self-assembly of peptide lipids in various solvents.[27,28]

Nanotubes (1 mg) with a hydrophobic surface in the presence of water (20 μL) were placed into an aluminum pan to facilitate differential scanning calorimetry (DSC) measurements. Results indicate an endothermic peak corresponding to a thermal phase transition (Supporting Information, Figure S5). The gel-to-liquid crystalline thermal phase transition temperature ($T_{g\text{-}l}$) was estimated to be 108 °C at high concentrations in a closed system. We already reported that a solid-state nanotube consisting of bilayer membranes converts in water into a fluid-state vesicle at temperatures above $T_{g\text{-}l}$.[21] In the present case, heat treatment of the nanotube (1 mg) in the presence of water (1 mL) was performed for 1 min at 85 °C, which is below the $T_{g\text{-}l}$ of 108 °C. The resultant nanotube was able to disperse in water and maintain its tubular morphology. Microscopic observations and spectroscopic measurements showed that the resultant nanotube was identical to the nanotube before heat treatment in terms of its morphological size and bilayer membrane structure. Heat treatment may induce rearrangement of the molecular packing of **1(18)** on the outermost surface of the nanotube through an inversion or flip-flop phenomenon.[29] Since a zeta-potential value (−38 mV) of the resultant nanotube in water were similar to that (−41 mV) of nanotubes having a hydrophilic surface covered with glucose headgroups of glycolipids,[30] the resultant nanotube should therefore have a hydrophilic surface covered with the glucose headgroups of **1(18)**.

4. Encapsulation of C60 in Hydrophobic Nanochannel

We have already reported that mixing lyophilized nanotubes, which have hydrophilic surfaces covered with the glucose headgroups of glycolipids, with aqueous solutions of hydrophilic, low-molecular-weight molecules, proteins, and metal nanoparticles enables the nanotubes to encapsulate such guests in their hydrophilic nanochannels via capillary force attraction.[15] In the present study, the nanotubes that were prepared in alcohols have hydrophobic surfaces covered with the alkyl-chain tail of **1(18)** and can encapsulate hydrophobic guests in the hydrophobic nanochannel via the same driving force. To encapsulate C60 in the hydrophobic nanochannel, we mixed the lyophilized nanotube (which was prepared in methanol) with a toluene solution of C60. The mixture was subjected to filtration through

a membrane with a pore size of 200 nm to collect the nanotube and to remove C60 present on the outside of the nanotube (Sample A). We also performed a control experiment without the use of capillary force attraction by mixing a toluene dispersion of the nanotube with the toluene solution of C60, and then removed the solvents (Sample B). The XRD pattern of sample B could be expressed as the summation of the XRD patterns of the nanotube and C60 (**Figure 3**); in contrast, the XRD pattern of sample A includes three remarkably weak and broadened peaks of C60 itself, an indication that C60 was homogeneously encapsulated in the hydrophobic nanochannel (**Figure 4**a).[31] We estimated the amount of C60 encapsulated in the nanotube (1.0 mg, [**1(18)**] = 2.37 μmol) to be 0.47 mg (0.65 μmol). In a previous study, we confirmed that low-molecular-weight molecules never enter into the solid-state bilayer membranes of the pre-formed nanotubes because the molecular packing is too tight and dense.[32]

The nanotube encapsulating C60 was smoothly transferred into water by the heat treatment described in the previous section, and an absorption spectroscopic analysis was performed on the nanotube while it was dispersed in water. The absorption spectrum derived from C60 was similar to that of the encapsulated C60 in the hydrophobic nanochannel of the nanotube while it was dispersed in *n*-hexane before the heat treatment. The hydrophobicity of the nanochannel was retained even though the hydrophobic outer surface was rearranged into a hydrophilic one after the heat treatment (Figure 4b). Furthermore, the fact that we observed in the longer wavelength region (400–550 nm) no broad peaks attributable to the self-aggregation of C60 within the bilayer membrane of liposomes[33] or the sheet (Supporting Information, Figure S6) implies that an incorporation and embedding of C60 into the bilayer membranes of the nanotube never occurred under these conditions. The nanotube was able to act as a fine nanocontainer for the dispersion of C60 in water (Figure 4b), even though both open ends of the hydrophobic nanochannel were exposed to water.

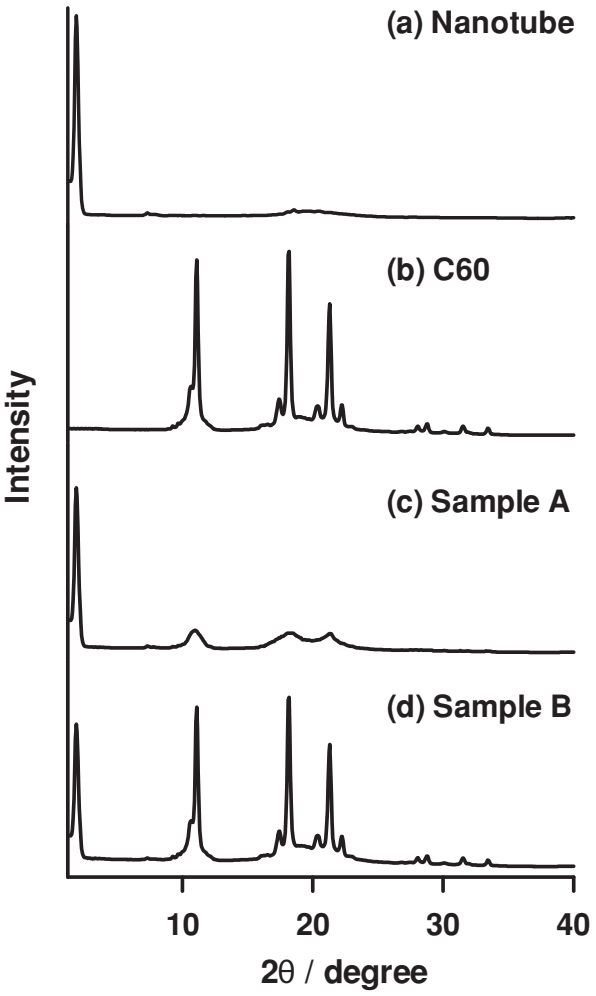

Figure 3. XRD patterns of a) the nanotube, b) C60, c) sample A: the nanotube encapsulating C60 in the nanochannel, and d) sample B: the nanotube + C60.

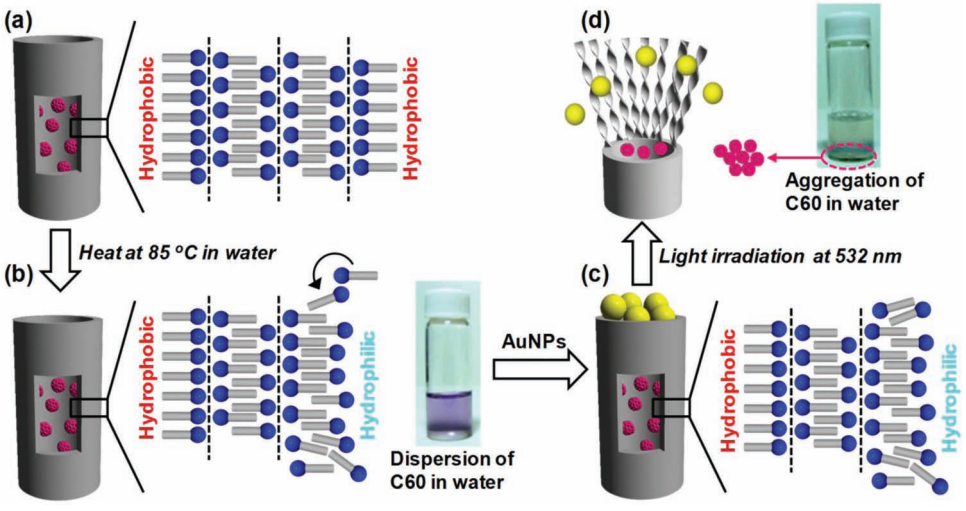

Figure 4. Schematic illustration of the dispersion/aggregation control of C60 in water by the encapsulation of C60 in the hydrophobic nanochannel and the release of the encapsulated C60 accompanied by the photothermal unfolding of the nanotube hybridized with AuNPs.

5. Dispersion/Aggregation Control of C60 by Hybridization of Photothermal AuNPs

Photothermal features of Au nanoparticles (AuNPs) have attracted much attention in the nano- and biomedical fields, because we can focally heat nanometer-to-micrometer-size targets by using irradiation as a remote stimulus.[34,35] Although the photothermal effect of the AuNPs evidenced by surface plasmon resonance (SPR) in the visible wavelength region (near 530 nm) is widely known to be lower than that of Au nanorods based on SPR in the near-infrared wavelength region (roughly 800–1000 nm), the AuNPs have been reported to be able to not only exhibit a strong cytotoxicity against cancer cells but also to dissolve thermally responsive gel matrices.[36] We expected that hybridization of the photothermal AuNPs to the nanotubes would lead to release of C60 accomplished by photothermally stimulated morphological transformation of the nanotubes.

We mixed the lyophilized nanotubes, which has a hydrophilic outer surface and hydrophobic nanochannel encapsulating C60, with a water dispersion of the AuNPs (Supporting Information, Figure S7, S8). The mixture was subjected to filtration through a membrane with a pore size of 200 nm to collect the nanotube and to remove any free AuNPs. Transmission electron microscopic (TEM) observations clearly showed that the AuNPs were hybridized in one end of the nanochannel (**Figure 5**a,b); such hybridized AuNPs were never observed in the other end or in the central part of the nanochannel.

We used a Nd-YAG laser (532 nm, 0.7 W) to irradiate for 5 min the water dispersion of the nanotube hybridized with the AuNPs and thereby induced an unfolding of the end where the AuNPs had been hybridized (Figure 5c,d). The temperature of the water dispersion was estimated to be about 37 °C during the irradiation (Supporting Information, Figure S9). We confirmed that the same irradiation of the water dispersion of the nanotube without AuNPs failed to induce a morphological transformation. The initiation of the unfolding process is ascribable to localized heating via the photothermal effect of the AuNPs. After the laser was turned off, the unfolding continued, and the nanotube was eventually transformed into narrow nanofibers.

The unfolding of the nanotube strongly influenced the dispersion/aggregation of C60. Without irradiation, C60 remained finely dispersed in the water by encapsulation in hydrophobic nanochannels (Figure 4b,c and **Figure 6**). In contrast, irradiation promoted the aggregation of C60 in the water as the result of compulsive release caused by disappearance of the nanochannel and unfolding of the nanotube (Figure 4d and Figure 6). The complete recovery of C60 as an aggregated precipitate implies that the nanofibers have no hydrophobic cavity for storing C60.

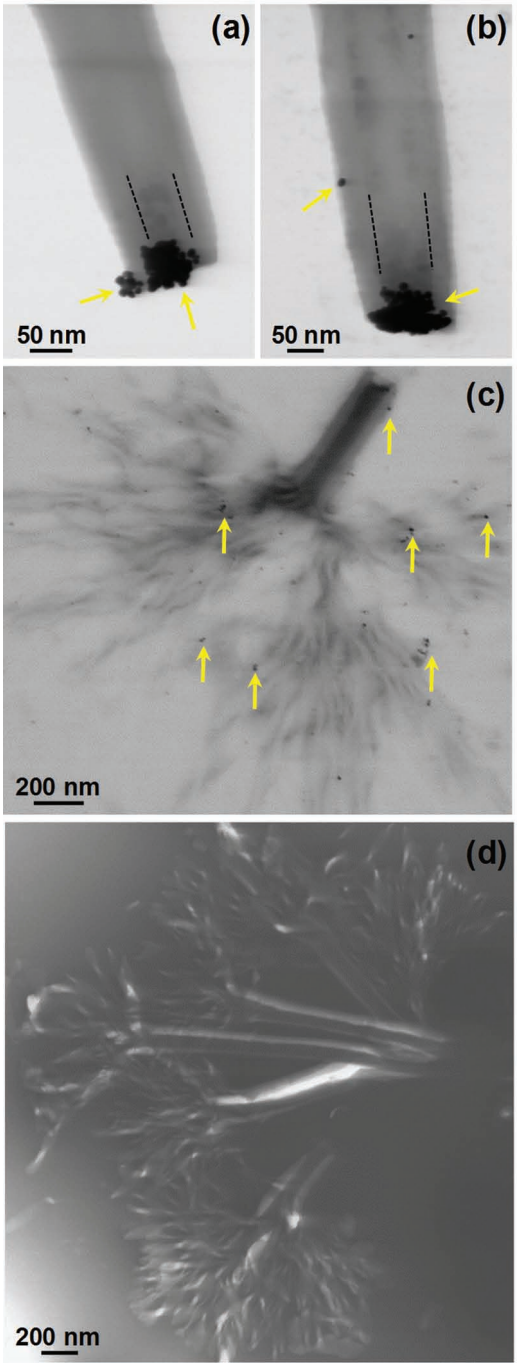

Figure 5. a,b) TEM images of the nanotube hybridized with AuNPs (yellow arrows). c) TEM image after irradiation of the unfolding of the nanotube hybridized with AuNPs. The nanochannel can be visualized as the relatively darker area by the encapsulation of C60. The black dots existing outside of the nanotube are the detached AuNPs (yellow arrows). d) TEM image after irradiation of the unfolding of the nanotube hybridized with AuNPs; the preparation was negatively stained with phosphotungstate.

6. Conclusions

We have succeeded in constructing nanotubes that have a hydrophilic outer surface and a hydrophobic nanochannel hybridized with AuNPs. The nanotubes were able to create a stable aqueous dispersion of C60 by encapsulating C60 in their nanochannels. The photothermal effect of the hybridized AuNPs induced unfolding of the nanotubes and a morphological transformation to nanofibers. The photothermal stimulation of the

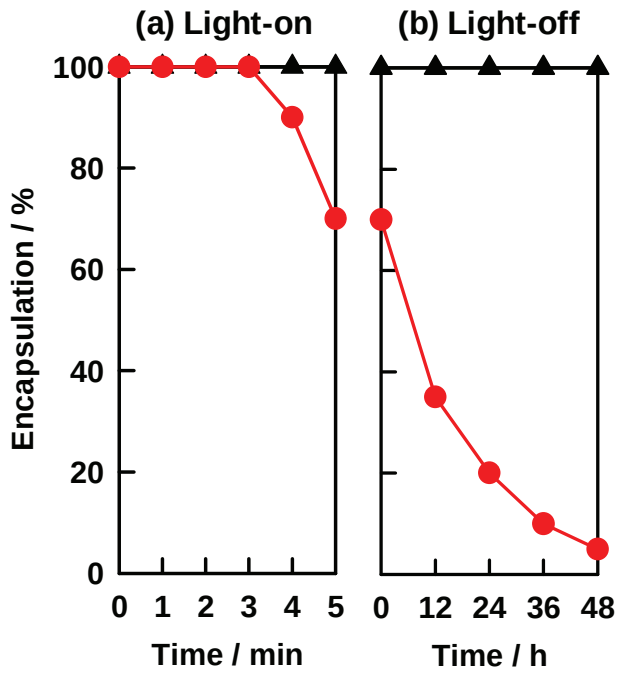

Figure 6. a) Time-dependence for the encapsulation ratio of C60 in the nanotube (black triangle plot) and the nanotube hybridized with the AuNPs (red circle plot) upon irradiation at 532 nm. b) Time-dependence for the encapsulation ratio of C60 in the nanotube (black triangle plot) and the nanotube hybridized with the AuNPs (red circle plot) after turning off the irradiation at 5 min. The precipitated C60 as the result of the release and aggregation was extracted into toluene, and the concentration of the extracted C60 was used for the calculation of the encapsulation ratio.

morphological transformation made possible precise control of the dispersion and aggregation of C60. The results of the present study should facilitate (1) biological, therapeutic, and cosmetic applications of C60 that address its functions as a photosensitizer and antioxidant[37–41] and (2) dispersion/aggregation control of other carbon nanomaterials, functional aromatic compounds, and drugs with low solubility.

7. Experimental Section

Synthesis of N-Alkaroyl-β-D-glucopyranosylamine ***1(n)***: The method of synthesizing **1(n)** was based on a previous report.[42] Stoichiometric mixtures of *D*-glucose and NH_4HCO_3 were stirred in a solution of 28% NH_4 at 40 °C for 24 h. The solvent was evaporated, and the residue was dissolved in methanol in the presence of 1 equivalent (eq.) of triethylamine. The methanol solution was added to a tetrahydrofuran solution containing 1 eq. of alkaroyl chloride. After the mixture was stirred at room temperature for 24 h, the solvent was evaporated. Crystallization was performed in methanol/water (1/1, v/v) and ethanol/ethyl acetate (1/1, v/v). The product was obtained as a white powder.

N-Stearoyl-β-D-glucopyranosylamine **1(18)**. Yield (35%). mp 179 °C. 1H NMR (400 MHz, DMSO-d_6, δ) 0.85 (t, 3H, 6.8 Hz, -CH_3), 1.23 (s, 28H, -CH_2-), 1.47 (t, 2H, 6.3 Hz, -$COCH_2CH_2$-), 2.04–2.11 (m, 2H, -$COCH_2$-), 2.99–3.11 (m, 3H, H-2, H-3, H-4), 3.12–3.20 (m, 1H, Glu H-5), 3.36–3.44 (m, 1H, H-6a), 3.62 (dd, 1H, 5.1 and 5.5 Hz, H-6b), 4.47 (t, 1H, 5.8 Hz, OH-6), 4.69 (t, 1H, 9.0 Hz, H-1), 4.80 (d, 1H, 5.5 Hz, OH), 4.86 (d, 1H, 5.1 Hz, OH), 4.95 (d, 1H, 4.4 Hz, OH), 8.24 (d, 1H, 8.9 Hz, -NHCO-). MALDI-TOF Mass (m/z): $[M + Na]^+$ calculated for $C_{24}H_{47}NO_6Na$: 445.34; found: 445.22.

N-Palmitoyl-β-D-glucopyranosylamine **1(16)**. Yield (32%). mp 176 °C. 1H NMR (400 MHz, DMSO-d_6, δ) 1.19 (s, 24H, -CH_2-), the other data are similar to those of **1(18)**. MALDI-TOF Mass (m/z): $[M + Na]^+$ calculated for $C_{22}H_{43}NO_6Na$: 439.29; found: 439.28.

N-Myristoyl-β-D-glucopyranosylamine **1(14)**. Yield (34%). mp 181 °C. 1H NMR (400 MHz, DMSO-d_6, δ) 1.19 (s, 20H, -CH_2-), the other data are similar to those of **1(18)**. MALDI-TOF Mass (m/z): $[M + Na]^+$ calculated for $C_{20}H_{39}NO_6Na$: 411.26; found: 411.21.

N-Lauroyl-β-D-glucopyranosylamine **1(12)**. Yield (39%). mp 189 °C. 1H NMR (400 MHz, DMSO-d_6, δ) 1.19 (s, 20H, -CH_2-), the other data are similar to those of **1(18)**. MALDI-TOF Mass (m/z): $[M + Na]^+$ calculated for $C_{18}H_{35}NO_6Na$: 383.46; found: 383.13.

Preparation of AuNPs: UV light at 254 nm (a 135 W low-pressure mercury lamp) irradiated a water/ethanol solution (4:1, v/v) of 10 mM $HAuCl_4$ for 2 h under an Ar atmosphere. Ethanol acted as a radical generator and proved to increase the photoreduction of $AuCl_4^-$. Dynamic light scattering (DLS) measurements showed that the AuNPs we obtained had diameters of about 10.5 nm (Supporting Information, Figure S7). Absorption spectroscopy revealed that the AuNPs had a typical surface plasmon resonance band (Supporting Information, Figure S8).

SEM and TEM Observations: The powder-state self-assemblies; the solvent dispersions of the self-assemblies; and those hybridized with AuNPs, encapsulating C60 or both were dropped onto grids and dried by a vacuum pump. SEM (Hitachi S-4800) and TEM (Hitachi H-7000) were operated at 30 and 75 keV, respectively.

FT-IR and XRD Measurements: The IR spectra of the lyophilized self-assemblies were measured with a Fourier transform IR spectrometer (JASCO FT-620) operated at 4 cm^{-1} resolution with an unpolarized beam and attenuated total reflection accessory system (Diamond MIRacle, horizontal ATR accessory with a diamond crystal prism, PIKE Technologies, USA) and a mercury cadmium telluride (MCT) detector. The XRD patterns of the lyophilized self-assemblies, C60, and the nanotube encapsulating C60 were measured with a Rigaku diffractometer (Type 4037) by using graded *d*-space elliptical side-by-side multilayer optics, monochromated Cu Kα radiation (40 kV, 30 mA), and an imaging plate (R-Axis IV). The exposure time was 5 min with a 150-mm camera length.

CD and UV-Visible Absorption Measurements: A spectropolarimeter (Jasco J-820) equipped with a temperature controller (Jasco PTC-423L) and a spectrophotometer (Hitachi U-3300) equipped with a temperature controller (Yamato BU150A) recorded the CD and absorption spectra, respectively.

DSC Measurements: The DSC profiles of the hydrated self-assemblies placed in an aluminum pan were recorded at 30–250 °C using a differential scanning calorimeter (DSC 6100, SEIKO) equipped with a nitrogen gas cooling unit. The peak temperature was taken as the phase transition temperature.

Supporting Information

Supporting Information is available from the Wiley Online Library or from the author.

Acknowledgements

This work was partly supported by a Grant-in-Aid for Young Scientists (B) (no. 24750143) from the Ministry of Education, Culture, Sports, Science and Technology (MEXT) and the Japan Society for the Promotion of Science (JSPS).

Received: July 31, 2012
Published online: October 22, 2012

[1] D. Wang, L. Chen, *Nano Lett.* **2007**, *7*, 1480.
[2] T. Kawauchi, J. Kumaki, A. Kitaura, K. Okoshi, H. Kusanagi, K. Kobayashi, T. Sugai, H. Shinohara, E. Yashima, *Angew. Chem.* **2008**, *120*, 525; *Angew. Chem. Int. Ed.* **2008**, *47*, 515.
[3] Y. Chen, B. Zhu, F. Zhang, Y. Han, Z. Bo, *Angew. Chem.* **2008**, *120*, 6104; *Angew. Chem. Int. Ed.* **2008**, *47*, 6015.
[4] Z. Zhang, Y. Che, R. A. Smaldone, M. Xu, B. R. Bunes, J. S. Moore, L. Zhang, *J. Am. Chem. Soc.* **2010**, *132*, 14113.
[5] S. S. Babu, H. Mohwald, T. Nakanishi, *Chem. Soc. Rev.* **2010**, *39*, 4021.
[6] M. Numata, S. Shinkai, *Chem. Commun.* **2011**, *47*, 1961.
[7] Z. Yao, K. C. Tam. *Macromol. Rapid Commun.* **2011**, *32*, 1863.
[8] S. Chen, Y. Jiang, Z. Wang, X. Zhang, L. Dai, M. Smet, *Langmuir* **2008**, *24*, 9233.
[9] T. Umeyama, K. Kawabata, N. Tezuka, Y. Matano, Y. Miyato, K. Matsushige, M. Tsujimoto, S. Isoda, M. Takano, H. Imahori, *Chem. Commun.* **2010**, *46*, 5969.
[10] W. Yi, A. Malkovskiy, Y. Xu, X.-Q. Wang, A. P. Sokolov, M. Lebron-Colon, M. A. Meador, Y. Pang, *Polymer* **2010**, *51*, 475.
[11] T. Shimizu, M. Masuda, H. Minamikawa, *Chem. Rev.* **2005**, *105*, 1401.
[12] X. Gao, H. Matsui, *Adv. Mater.* **2005**, *17*, 2037.
[13] E. Gazit, *Chem. Soc. Rev.* **2007**, *36*, 1263.
[14] J. Fang, *J. Mater. Chem.* **2007**, *17*, 3479.
[15] N. Kameta, H. Minamikawa, T. Shimizu, *Soft Matter* **2011**, *7*, 4539.
[16] N. Kameta, A. Tanaka, H. Akiyama, H. Minamikawa, M. Masuda, T. Shimizu, *Chem. Eur. J.* **2011**, *17*, 5251.
[17] R. G. Snyder, S. L. Hsu, S. Krimm, *Spectrochim. Acta, Part A* **1978**, *34*, 395.
[18] R. G. Snyder, H. L. Strauss, C. A. J. Elliger, *J. Phys. Chem.* **1982**, *86*, 5145.
[19] N. Garti, K. Sato, *Crystallization and Polymorphism of Fats and Fatty Acids,* Marcel Dekker, New York **1988**, pp. 139–187.
[20] N. Yamada, K. Okuyama, T. Serizawa, M. Kawasaki, S. Oshima, *J. Chem. Soc., Perkin Trans. 2* **1996**, *12*, 2707.
[21] S. Kamiya, H. Minamikawa, J. H. Jung, B. Yang, M. Masuda, T. Shimizu, *Langmuir* **2005**, *21*, 743.
[22] F. J. M. Hoeben, P. Jonkheijm, E. W. Meijer, A. P. H. J. Schenning, *Chem. Rev.* **2005**, *105*, 1491.
[23] T. F. A. De Greef, M. M. J. Smulders, M. Wolffs, A. P. H. J. Schenning, R. P. Sijbesma, E. W. Meijer, *Chem. Rev.* **2009**, *109*, 5687.
[24] M. S. Spector, J. V. Selinger, J. M. Schnur, in *Topics in Stereochemistry*, *Vol. 24* (Eds: M. M. Green, R. J. M. Nolte, E. W. Meijer), Wiley, New York **2003**, pp 281–372.
[25] M. S. Spector, R. R. Price, J. M. Schnur, *Adv. Mater.* **1999**, *11*, 337.
[26] M. S. Spector, K. R. K. Easwaran, G. Jyotshi, J. V. Selinger, A. Singh, J. M. Schnur, *Proc. Natl. Acad. Sci. USA* **1996**, *93*, 12943.
[27] C. Boettcher, B. Schade, J.-H. Fuhrhop, *Langmuir* **2001**, *17*, 873.
[28] M. Kogiso, M. Aoyagi, M. Asakawa, T. Shimizu, *Soft Matter* **2010**, *6*, 4528.
[29] J.-H. Fuhrhop, T. Wang, *Chem. Rev.* **2004**, *104*, 2901.
[30] Y. G. Han, M. Aoyagi, M. Asakawa, T. Shimizu, *Appl. Mater. Interfaces* **2012**, *4*, 2439.
[31] S. Minakata, R. Tsuruoka, M. Komatsu, *J. Am. Chem. Soc.* **2008**, *130*, 1536.
[32] N. Kameta, M. Asakawa, M. Masuda, T. Shimizu, *Soft Matter* **2011**, *7*, 85.
[33] A. Ikeda, K. Kiguchi, T. Shigematsu, K. Nobusawa, J. Kikuchi, M. Akiyama, *Chem. Commun.* **2011**, *47*, 12095.
[34] M.-C. Daniel, D. Astruc, *Chem. Rev.* **2004**, *104*, 293.
[35] M. Hu, J. Chen, Z. Y. Li, L. Au, G. V. Hartland, X. Li, M. Marquez, Y. Xia, *Chem. Soc. Rev.* **2006**, *35*, 1084.
[36] C. Kojima, S.-H. Cho, E. Higuchi, *Res. Chem. Intermed.* **2012**, *38*, 1279.
[37] J. Lee, S. Mahendra, P. J. J. Alvarez, *ACS Nano* **2010**, *4*, 3580.
[38] S. Kato, H. Taira, H. Aoshima, Y. Saitoh, N. Miwa, *J. Nanosci. Nanotechnol.* **2010**, *10*, 6769.
[39] Y. Ishida, T. Fujii, K. Oka, D. Takahashi, K. Toshima, *Chem. Asian J.* **2011**, *6*, 2312.
[40] L. Yang, L. Zhang, T. J. Webster, *Nanomedicine* **2011**, *6*, 1231.
[41] L S. Yanoa, S. Hiroharab, M. Obatac, Y. Hagiyad, S. Ogurad, A. Ikedab, H. Kataokae, M. Tanakae, T. Johe, *J. Photochem. Photobiol., B* **2011**, *12*, 46.
[42] A. Lubineau, J. Auge, B. Drouillat, *Carbohydr. Res.* **1995**, *266*, 211.